



HAL
open science

Martini 3 Coarse-Grained Model for Type III Deep Eutectic Solvents: Thermodynamic, Structural, and Extraction Properties

Petteri Vainikka, Sebastian Thallmair, Paulo Cesar Telles Souza, Siewert Marrink

► **To cite this version:**

Petteri Vainikka, Sebastian Thallmair, Paulo Cesar Telles Souza, Siewert Marrink. Martini 3 Coarse-Grained Model for Type III Deep Eutectic Solvents: Thermodynamic, Structural, and Extraction Properties. ACS Sustainable Chemistry & Engineering, In press, 9 (51), pp.17338-17350. 10.1021/acssuschemeng.1c06521 . hal-03864619

HAL Id: hal-03864619

<https://cnrs.hal.science/hal-03864619>

Submitted on 25 Nov 2022

HAL is a multi-disciplinary open access archive for the deposit and dissemination of scientific research documents, whether they are published or not. The documents may come from teaching and research institutions in France or abroad, or from public or private research centers.

L'archive ouverte pluridisciplinaire **HAL**, est destinée au dépôt et à la diffusion de documents scientifiques de niveau recherche, publiés ou non, émanant des établissements d'enseignement et de recherche français ou étrangers, des laboratoires publics ou privés.

Martini 3 coarse-grained model for type III deep eutectic solvents: Thermodynamic, structural, and extraction properties

Petteri A. Vainikka,^{†,‡} Sebastian Thallmair,^{‡,¶} Paulo C. T. Souza,^{‡,§} and Siewert J. Marrink^{*,†,‡}

[†]*Zernike Institute for Advanced Materials, University of Groningen, Nijenborgh 4, 9747 AG Groningen, The Netherlands*

[‡]*Groningen Biomolecular Sciences and Biotechnology Institute, University of Groningen, Nijenborgh 7, 9747 AG Groningen, The Netherlands*

[¶]*Frankfurt Institute for Advanced Studies, Ruth-Moufang-Str. 1, 60438 Frankfurt am Main, Germany*

[§]*Molecular Microbiology and Structural Biochemistry (MMSB, UMR 5086), CNRS, University of Lyon, Lyon, France*

E-mail: s.j.marrink@rug.nl

Abstract

Deep eutectic solvents (DESs) are a more environmentally friendly, cost-effective, and recyclable alternative for ionic liquids. Since the number of possible deep eutectic solvents is very large, there are needs for effective methods to predict the physico-chemical nature of possible new deep eutectic solvents that are not met by the currently available models. Here, we have built coarse-grained models for a few well-known and actively studied deep eutectic solvents using the recently published Martini 3 force field. Molecular dynamics simulations demonstrate that our models predict the properties of these particular DESs with an acceptable accuracy, and are capable of capturing known liquid-liquid extraction processes as well as morphological shape changes of surfactant aggregates. Our coarse-grained approach is novel in the study of DESs, opening new possibilities for rapid screening of new DESs and their properties.

Introduction

Deep eutectic solvent (DES) is a name for a class of solvents which are typically formed as a result of mixing Brønsted or Lewis acids with hydrogen bond acceptors (HBA).^{1,2} Within a correct molar ratio, which varies depending on the thermodynamic properties of the pure compounds forming the DES, they form an eutectic mixture, manifested by a significant depression in the freezing point, allowing them to remain liquid at room temperature.³ Although they are primarily synthesized for laboratory and industrial use, they are also present in nature: Recent work suggests that so called 'natural DESs' (NADESs) could form a separate liquid phase inside mammalian and plant cells, contributing to both the cellular metabolism, and the survivability of the cell.⁴ Our work focuses primarily on type III DESs, which are formed by mixing a quaternary ammonium salt with a hydrogen bond donor.^{2,5} Care should be taken when considering whether or not a solvent is indeed a 'deep eutectic' solvent: The simple presence of a eutectic point, which is ubiquitous in mixtures, or the ability to form hydrogen bonds is not enough.^{3,6} The work of Martins *et al.*³ is recommended for further consideration of the topic.

Publications related to using eutectic mixtures as substrates in enzymatic catalysis can be found in mid-1990s,^{7,8} but the wide range of their potential uses as solvents was not realized until the early 2000s. In 2003 Andrew Abbott and colleagues reported the synthesis of a DES by mixing choline chloride and urea.⁹ This is, to the extent of the authors knowledge, the first use of the term 'deep eutectic', coined in order to differentiate between ionic liquids (ILs) and DESs. In the following year Abbott *et al.* demonstrated the synthesis of multiple DESs using quaternary ammonium salts and carboxylic acids.¹⁰

This work was among the first to highlight multiple, potentially important and lucrative properties of DESs: They share many of the coveted properties of ILs, such as wide liquid ranges, very low vapour pressures, non-flammability, and applicability in various processes relevant to both academia and industry.^{6,11-13} Contrary to ILs, preparation of DESs has optimal atom economy,¹³ they require comparatively little purification as the purity of any DES

is directly ordained by the purity of the compounds from which it was generated from,^{3,14} and most materials used in their formulation are cheap and readily available.¹⁴⁻¹⁶ Additionally, by carefully selecting the precursors, DESs can be made environmentally friendly¹⁷ and/or easily recyclable.¹⁸

Although the total number of possible DESs is unknowable, and will likely to remain so until the community has come to an agreement on how to classify a solvent as a DES, current works have demonstrated that the growing amount of existing DESs is turning comprehensive experimental mapping of their properties and behaviour less and less feasible.^{19,20} This has prompted the use of theoretical and computational methods in studying the properties and predicting new possible DESs. These methods include, but are not limited to, molecular dynamics simulations,²¹⁻²⁶ classical thermodynamic models such as group contribution methods,^{19,27,28} and quantum chemical calculations.²⁹⁻³² While some group contribution methods (COSMO-RS, UNIFAC, and others) are being used to predict properties of possible new DESs, a significant portion of publications related to these methods focus on correlating experimental data from type III DESs.³³

The theoretical studies of the structure and dynamics of DESs rely on all-atom (AA) molecular dynamics simulations. These simulations allow for great accuracy but are resource intensive, making proper sampling in larger or dynamically slower systems more cumbersome. As an alternative to AA models, coarse-grained (CG) models have found widespread applications.^{34,35} By replacing groups of atoms into effective interaction sites, so-called CG beads, a large computational speedup is obtained at the cost of a somewhat reduced accuracy.³⁶ One of the most popular CG models is the Martini force field,³⁷ in which 2-4 heavy atoms and associated hydrogens are united into CG beads.

Martini has been successfully employed in studies of various biologically relevant systems³⁸⁻⁴² and more recently in material sciences.⁴³⁻⁴⁶ One key reason for the high applicability of Martini has to do with the top-down process by which it was parameterized,^{37,47} placing focus on matching thermodynamic parameters provides a level of transferability, en-

asuring at least some level of compatibility between newly parameterized models and existing models, as has been demonstrated in recent work with ILs.⁴³ This fact encouraged us to create the first Martini DES models, namely choline chloride - urea, tetrabutylammonium chloride - decanoic acid, and DL-menthol -acetic acid, based on the latest version of the force field (Martini 3.0⁴⁷). With the parameterization of these models, not only could we study the properties of these solvents themselves, but also their interactions with the wide array of pre-existing Martini models. The latter possibility opens, among other things, a completely new realm of temporal and spatial resolutions for studies of DES liquid-liquid extraction (LLE) processes with molecular dynamics, as will be demonstrated later in this document.

The paper is structured as follows: We first describe the parameterization and reasoning behind these models. This is followed with a comparison of the properties of these DESs against experimental data and AA simulations. Finally, we demonstrate the performance of the new models with test cases in which we evaluate the performance of our models against experimental data in more complex environments, namely the extraction of aromatic compounds from oil and water, and the self-assembly of surfactants.

Methods

Computational Details

All simulations were performed with GROMACS 2018.1⁴⁸⁻⁵⁴ using the Bussi-Donadio-Parrinello thermostat (V-rescale).⁵⁵ Simulation pressures were controlled with the Berendsen barostat⁵⁶ during equilibration, and with the Parrinello-Rahman barostat⁵⁷ during production simulations. Constraints, where applied, were solved using LINCS,⁵⁸ with a LINCS order of 4. All-atom simulations were run with a 2 fs timestep, while the CG simulations used a 20 fs timestep. Electrostatic interactions in AA and CG systems were computed using the smooth particle mesh Ewald (PME) method,⁵⁹ although all CG systems were also tested with the Reaction-Field method. All atom models were based on the CHARMM36 force field,^{60,61}

released in March 2019 and ported for GROMACS by Bjelkmar *et al.*⁶²

Simulation setup

AA reference simulations of individual DES components were performed by placing the solute in question inside a 3.5 nm³ cubic box and solvating the system with TIP3P water. In case the solute had a net charge, a counterion was used to keep the system neutral. After energy minimization, using steepest descend algorithm in GROMACS, the system was equilibrated first in a NVT ensemble at ambient temperature for 1 ns, then in a NPT ensemble and ambient temperature and pressure for 1 ns, followed by a production simulation in the same ensemble for 300 ns. The routine for CG models consisted of the same energy minimization step, followed by four equilibration steps with timesteps of 1, 2, 10, and 20 fs respectively. The equilibration simulations totalled to 80 ns, and were followed by a 1 μ s production simulation. Both the equilibration and the production simulations were performed with a NPT ensemble.

CG simulations of pure DESs were set up in two ways; by either randomly placing each molecule within the simulation volume as demonstrated in Figure 1, or by combining two separate phases formed in two separate simulations. Energy minimization and equilibration for every CG system followed the same routine described above. All LLE simulations were set up by randomly placing molecules in the simulation volume. The detailed compositions of the systems are given in Supplementary Information section 5.

A special case was made for testing the properties of solid tetrabutylammonium chloride (TBAC). A unit cell of the crystal structure was obtained from the Cambridge Crystallographic Data Centre (CSD Entry: XUBGIN) and packed in to a 5 \times 5 \times 5 crystal using Mercury.^{63–67} The atomistic crystal structure was subsequently forward-mapped using PyCGTOOL,⁶⁸ and simulated with anisotropic pressure coupling both, as a pure crystal and as a crystal immersed in disordered TBAC. The system setup is illustrated in Figure 2.

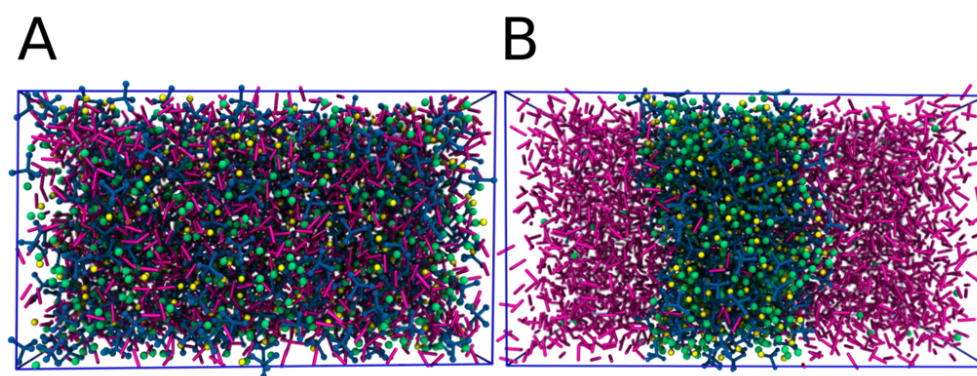


Figure 1: Example system setup for biphasic DES systems. (A) Random configuration starting structure. (B) Final self-assembled biphasic structure. The mixture shown in these images are composed of tetrabutylammonium chloride (blue and yellow, respectively), acetic acid (green), and octane (purple).

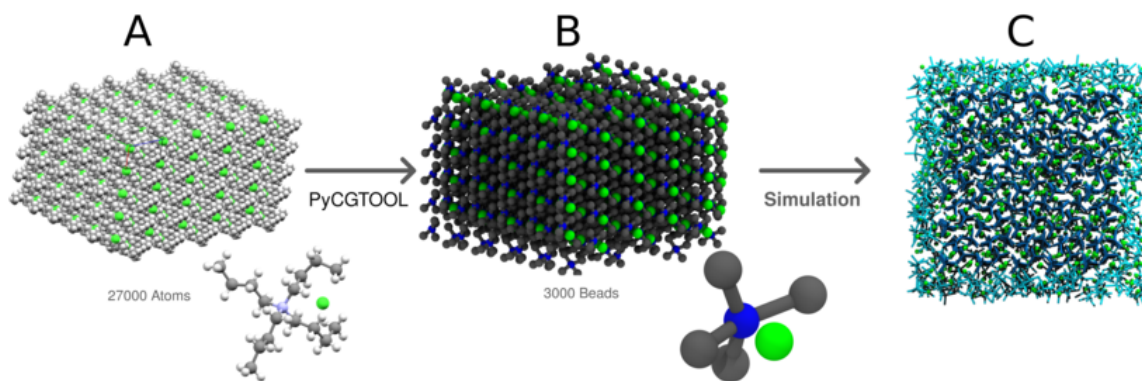


Figure 2: System setup for TBAC crystal simulations. (A) Atomistic structure. (B) CG structure obtained by forward mapping using PyCGTOOL. (C) Crystalline TBAC (dark blue) immersed in disordered TBAC (cyan).

Parameterization

Initial CG models presented in this work were parameterized using a more recent development version of Martini 3 open-beta.⁶⁹ All systems presented here were tested again with the published parameters of Martini 3,⁴⁷ and all reported values are from simulations with these parameters. Here we only give a cursory account of the parameterization process. A more detailed description of parameterizing small molecules for the Martini 3 force field can be found in the recent work of Alessandri *et al.*⁷⁰

CHARMM36 and GROMACS compatible AA starting structures and topologies were obtained from SwissParam tool,⁷¹ and used as a basis for determining bonded interactions for the corresponding CG model. Being aware of the fact that SwissParam output is primarily meant for molecular docking and other applications in which high-level details are not the highest priority,⁷¹ we compared the bonded parameters produced by SwissParam to those produced by Q-Force,⁷² a QM based toolkit which derives bonded parameters through Hessian fitting. Comparison of the two predicted topologies was carried by simulating both models for 250 ns at the AA level, after which they were mapped to the corresponding CG structure using the centre-of-geometry (COG) mapping method. Comparing how the difference in AA bonded terms carries out to the final CG model, we found the average deviation between the bond lengths in the two CG models to be around 2.22%, while the angles deviated by 2.73%. Results of these comparisons are presented more thoroughly in Supplementary Information section 2. Based on these findings, we concluded that the possible errors present in the bonded terms predicted by SwissParam are at a tolerable level.

Following the COG mapping and assignment of bonded interactions between CG beads, the chemical nature of each moiety (represented by a bead) was evaluated and a relevant bead type was assigned to it. Fit of the bonded parameters (bond lengths, reference angles etc.) was improved by iteratively changing the parameters until a reasonable fit between the mapped AA models and the CG models was achieved. Finally, the shape and occupied volume of the CG model was semi-quantitatively compared to its atomistic counterpart

via computation of the solvent accessible surface area (SASA) and the resulting Connolly-surface. We used two sets of approximate values for atomistic radii; the default values distributed with most GROMACS versions,⁷³ and a more recent set from Rowland *et al.*⁷⁴ These results are reported in the Supplementary Information section 3. Partial charges of choline, tetrabutylammonium and urea were derived using the CHelpG scheme,⁷⁵ computed with Gaussian16 software.⁷⁶

Free energy estimates and partition coefficients

Assessing the correctness of non-bonded parameters, modelled via the Lennard-Jones and the Coulomb interactions, for individual CG models was performed by comparing experimentally and theoretically derived water-octanol partition coefficients ($\log P$) to values computed for our models by thermodynamic integration (TI). The TI routine is described in full detail in the Supplementary Information section 4.

Thermal expansion coefficient

We estimated α , the thermal expansion coefficient of each DES studied, and compared the results against values reported in literature wherever available. α is given by:

$$\alpha = -\left(\frac{\partial \ln \rho}{\partial T}\right)_p \tag{1}$$

where ρ is the density of the evaluated system, T is temperature, and p is pressure. In order to evaluate α , each DES was simulated three times as either dry ($\chi_{H_2O} = 0$) or wet ($\chi_{H_2O} = 0.1$) within a temperature range of 288 - 338 K. The range was scanned in intervals of 5 K. In the case of DL-menthol - acetic acid DES the upper limit of the temperature range was extended from 338 K to 353 K due to available experimental data of densities at higher temperatures.

Radial distribution functions

Liquid structures of CG DES systems were studied by comparing them against their atomistic counterparts by evaluating the radial distribution functions of key component pairs: hydrogen bond acceptor (HBA) - HBD, HBA - water, and HBA - counterion. Bin volume and density were normalized, and the evaluation was performed on the centre-of-mass of each component, in order to obtain comparable results between the two resolutions.

Extraction efficiency

In order to compare the results from our LLE simulations to experiment, we computed the extraction efficiencies for each system. We calculated the extraction efficiency with:

$$\frac{f_0 - f_1}{f_0} \times 100\% \tag{2}$$

where f is the number density of the solute which is to be extracted. f_0 refers to the initial density of the solute within the solvent phase at the start of the process and f_1 to the density of the solute in the same phase after the process. We computed these values using the density profile of our system (typically along the z -axis), and by evaluating the number density of the target compound within the bulk of both phases, ignoring the density within the interface region.

Asphericity and shape estimations

The last test case presented in this study focused on sodium dodecyl sulfate micelles (SDS), and their conformations when solvated in water or choline chloride - urea DES. The lengths of the micelles were computed from a distance matrix consisting of positions of all SDS molecules at every point in time. The radius of gyration and moments of inertia were computed using built-in GROMACS tools. Asphericity was computed using the scheme published by Dima *et al.*,⁷⁷ which has been implemented in the MDAnalysis toolkit.^{78,79}

Viscosity calculation

Shear viscosities of the simulated DESs were estimated with the Einstein relation, which is implemented in the *gmx energy* tool, available in GROMACS:⁴⁸

$$\eta = \frac{1}{2} \frac{V}{k_B T} \lim_{t \rightarrow \infty} \frac{d}{dt} \left\langle \left(\int_{t_0}^{t_0+t} P_{xz}(t') dt' \right)^2 \right\rangle_{t_0} \quad (3)$$

In the equation above, V is the system volume and P_{xz} is the average of the three off-diagonal elements of the pressure tensor.

Following the approach reported by Maginn *et al.*,⁸⁰ we evaluated the viscosity of each DES at eight equally spaced temperatures, ranging from 283, 293, ... , 353 K. A hundred replicas were run for each temperature, totaling 2400 separate simulations. Each system was equilibrated as described previously, and simulated in a NVT ensemble for 2.5 nanoseconds with a timestep of 5 fs.

Surface tension calculation

To assess the volatility of our DES models, and the correctness of our intermolecular interactions, we computed surface tension (γ) given by:

$$\gamma = \frac{L_z}{2} \left\langle P_{zz} - \frac{P_{xx} + P_{yy}}{2} \right\rangle \quad (4)$$

where L_z is the length of the z-axis, P_{xx}, P_{yy} , and P_{zz} are the diagonal components of the pressure tensor, corresponding to the X, Y, and Z-axis, respectively. The factor 1/2 comes from the number of interfaces present in the simulation, which was two in our systems. Evaluation of the surface tension of each DES was done by equilibrating a system as described previously, and then elongating Z-axis such that over 66 % of the simulation volume consists of vacuum. For each DES, 20 replicas were simulated in 298 K for 200 nanoseconds, after which the surface tension was computed.

Results

Construction of DES topologies

Our study began with the parameterization of five new CG models of hydrogen bond acceptors (HBAs) and donors (HBDs), allowing for the simulation of three DESs; the hydrophobic tetrabutylammonium chloride - decanoic acid DES, the hydrophilic choline chloride - urea DES, and the DL-menthol - acetic acid NADES. Acetic acid had been previously parameterized for Martini 3 by Souza *et al.*⁴⁷ In addition, we parameterized molecules for the application of these DESs, namely benzothiophene, 2-methylthiophene, imidacloprid and dodecyl sulfate. CG models of all the components with their respective chemical structures are given in Figure 3. Full details of all newly parameterized models can be found in the Supplementary Information section 1.

Most of the topologies presented here can be derived simply by following the established rules, which can be found in the recent Martini 3 paper,⁴⁷ or online at cgmartini.nl in the 'Tutorials' section. Since explicit hydrogen bonding is not possible at the CG resolution, these models require the use of the hydrogen bond donor and acceptor labels (d and a , respectively), which capture the hydrogen bonding propensities of the underlying chemical fragments in an effective manner. In the case of tetrabutylammonium cation, the standard mapping scheme resulted in the central nitrogen and first carbons of each four butyl chains being mapped in to a single regular Q-bead, carrying a positive unit charge. The remaining carbons on each butyl chain were mapped to SC3 beads, which in turn shielded the central Q-bead and severely hindered electrostatic interactions between the charged Q-bead and the counterion. To remedy this, we constructed four virtual sites in tetragonal arrangement around the central bead and divided the charge between these four sites, and the central bead. This arrangement was found to significantly improve the interaction between TBA⁺ and Cl⁻, and allowed the central bead to be mapped to a more characteristic N2q-bead, due to the decreased partial charge on that bead. Further details are given in the Supplementary

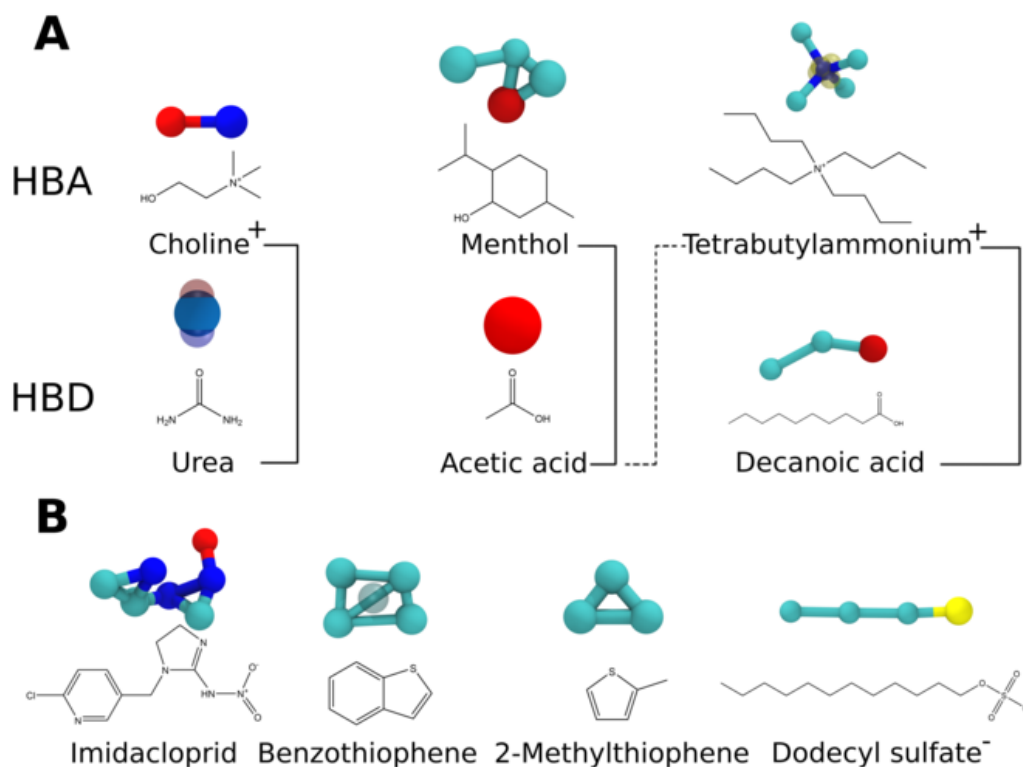


Figure 3: DES compounds used in this study. (A) DES forming compounds, with the hydrogen bond acceptors (HBAs) on the top and hydrogen bond donors (HBDs) on the bottom. Compounds connected with a solid black line indicate DESs created in this study. A dashed line is drawn between TBA and AcAc, indicating their use in extraction of MTP and BTP. (B) Target compounds used in applications, which are described later in this paper. Red colour indicates a P-type bead, cyan corresponds to a C-type bead (with one exception, see SI section 1.8 for more information), blue is used for N-type beads, and yellow indicates a Q-type bead. Transparent beads are virtual sites or non-interacting U beads, which are described in more detail in the SI section 1.

Information section 1.1.

Following the general rules for mapping, urea was originally mapped as a single SP2 bead. However, this would have made it almost indistinguishable from methanol, and completely indistinguishable from acetic acid. This was circumnavigated by placing two non-interacting U-beads were at 0.1 nm from the SP2 bead which were assigned opposite and equal partial charges in order to at least partially capture the highly polar nature of the compound. Further details are given in the Supplementary Information section 1.5.

Validation of the DES models

Density, thermal expansion coefficients, viscosity and surface tension

Densities of pure DESs were evaluated within a temperature range of 288, 293, 298... 338 K and compared against experimentally available data. Both, a completely dry, and water saturated systems were simulated in three replicas, separately for each DES. The resulting density curves as a function of temperature are given in section 6 of the Supplementary Information. Generally the Martini 3 models tend to overestimate the density by 5 to 10 %. The temperature dependency of the densities are captured reasonably well, as is evident from the thermal expansion coefficients (α) presented in Table 1.

Table 1: Thermal Expansion Coefficients of DESs studied in this work.

Thermal Expansion Coefficients (α)				
DES	Water	Martini 3 ($\times 10^{-3} K^{-1}$)	Experiment ($\times 10^{-3} K^{-1}$)	Reference
TBAC - DecA	Dry	0.929 ± 0.004	1.040 ± 0.008	Ref. ⁸¹
TBAC - DecA	Wet	0.931 ± 0.004	1.060 ± 0.005	Ref. ⁸¹
			0.696 ± 0.002	Ref. ⁸²
Menthol - AcAc	Dry	1.671 ± 0.024	0.925 ± 0.010	Ref. ⁸³
Menthol - AcAc	Wet	1.637 ± 0.026	0.886 ± 0.009	Ref. ⁸³
Chol. Cl - urea	Dry	0.617 ± 0.004	0.458 ± 0.006	Ref. ⁸⁴
			0.533 ± 0.016	Ref. ⁸⁵
			0.436 ± 0.010	Ref. ⁸⁶
Chol. Cl - urea	Wet	0.626 ± 0.002	0.531 ± 0.016	Ref. ⁸⁵
			0.449 ± 0.001	Ref. ⁸⁶

Predicted shear viscosities were systematically lower than those reported from experiment,^{85,87,88} but some general trends were captured. Further information is given in the Supplementary Information section 7. Predicted surface tensions match experimental values⁸⁹⁻⁹¹ relatively well, with all values being within $20 \text{ mN} \times \text{m}^{-1}$ from their experimental counterparts. Further information is given in the Supplementary Information section 8.

Partition coefficients

A key hallmark of the Martini model is reproduction of partition coefficients. To validate our DES models in this regard, water-octanol partition coefficients ($\log P$) were computed using TI, and matched against experimental and predicted values with the exception of dodecyl sulfate for which no experimental $\log P$ values could be found. Results are shown graphically in Figure 4, and the corresponding data is given in Table 2. On average, the $\log P$ values of the Martini 3 models differed from experimental values by 0.2 $\log P$ units, corresponding roughly to half $k_B T$. Choline-cation was the only significant outlier, differing by roughly one $\log P$ unit from the experimental value.

Table 2: Log P values obtained with Martini 3, experimental values with their respective references, and predicted values with the software they were predicted with. [†] This value is obtained through QM computation, and thus it is not a true experimental value. However, the approach is built on higher level of theory than is typically used for predicting $\log P$ values. See reference nr. 92, p. 123 for more details. Simulation results are at 310 K; the temperature of the experimental measurements are not explicitly defined, and are assumed to be ambient.

Water - octanol partition coefficients					
Compound	Martini 3	Experimental	Reference	Predicted	Software
TBA ⁺	4.47 ± 0.06	4.51 [†]	Ref. ⁹²	3.54	AlogPs
DecA	4.52 ± 0.02	4.09	Ref. ⁹³	4.10	XLogP3
Menthol	2.73 ± 0.17	3.03	Ref. ⁹⁴	3.40	XLogP3
Choline ⁺	-2.95 ± 0.04	-3.77	Ref. ⁹⁵	-3.60	AlogPs
Urea	-1.23 ± 0.04	-1.54	Ref. ⁹⁶	-1.40	ChemAxon
Benzothiophene	2.73 ± 0.03	3.12	Ref. ⁹³	3.10	XLogP3
2-methylthiophene	2.61 ± 0.05	2.33	Ref. ⁹⁷	2.30	XLogP3
Imidacloprid	1.07 ± 0.07	0.57	Ref. ⁹⁸	0.41	KowWin
Dodecyl sulfate ⁻	4.63 ± 0.11	N/A		4.42	ChemAxon

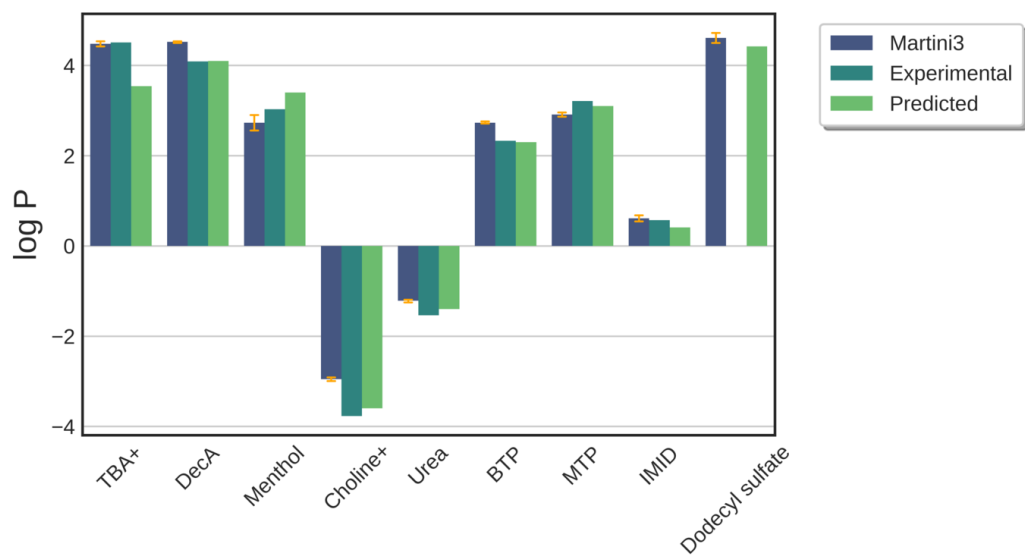


Figure 4: Computed, experimental, and predicted log P values of the 9 compounds modelled for this study.

Liquid structure

Another key factor in assessing the correctness of our model was to compare the liquid structure within DESs against structures predicted by AA simulations. We placed our focus on radial distribution functions (RDFs) of the quaternary ammonium cations with respect to their counterions, water and the HBD. The results, as shown in Figure 5, indicate that the RDFs are in a good agreement with each other.

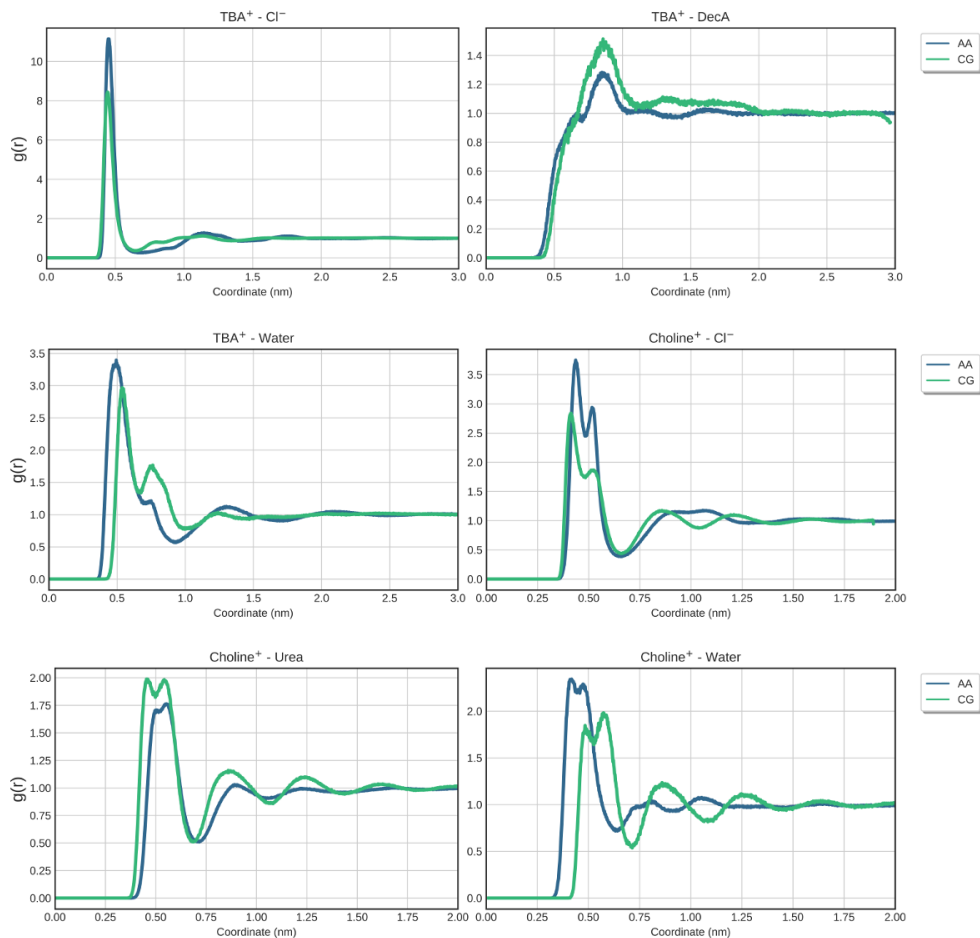


Figure 5: Radial distribution functions of TBA⁺ - Cl⁻ and Choline⁺ - Cl⁻ on both, coarse-grained and atomistic level.

Properties of solid TBAC

Most DES components remain in a solid state in ambient conditions, with some having melting points well above room temperature. Although the Martini model is primarily parameterized for modelling systems in the liquid state, we investigated whether or not a solid state can actually be reproduced with our DES topologies. As a test case, we selected a common DES component, TBAC, due to the availability of information about its crystalline structure and its common use in DES studies. Melting point of crystalline TBAC was estimated by simulating a single TBAC crystal immersed in an equal amount of fluid TBAC, in temperatures ranging from 250 to 315 K, with temperature increments of 5 K. From these simulations we expect to see the crystal phase growing below the melting temperature, and a fluid phase above the melting point. Each temperature was simulated three times for 300 ns, with the exception of 315 K, which results in a rather unstable system, due to the anisotropic pressure coupling. For each simulation, we computed the diffusion coefficient of both ions (TBA^+ and Cl^-), since partial and complete melting of the system is easily observed from these values. While computing the MSD, no distinction was made between the compounds originally residing in the crystal and in the fluid phase. Results from this analysis are given in Figure 6. Experimentally the melting point has been estimated to be 310 ± 1 K,⁹⁹ and our model predicts the melting temperature to be around 300 to 305 K, at which point we notice sharp increases in the magnitude of the diffusion coefficients, from 10^{-5} to 10^0 cm^2/s , as well as in the overall cell volume (not shown). This increase signals the formation of a fluid phase as can also be seen in the graphical snapshots in Figure 6.

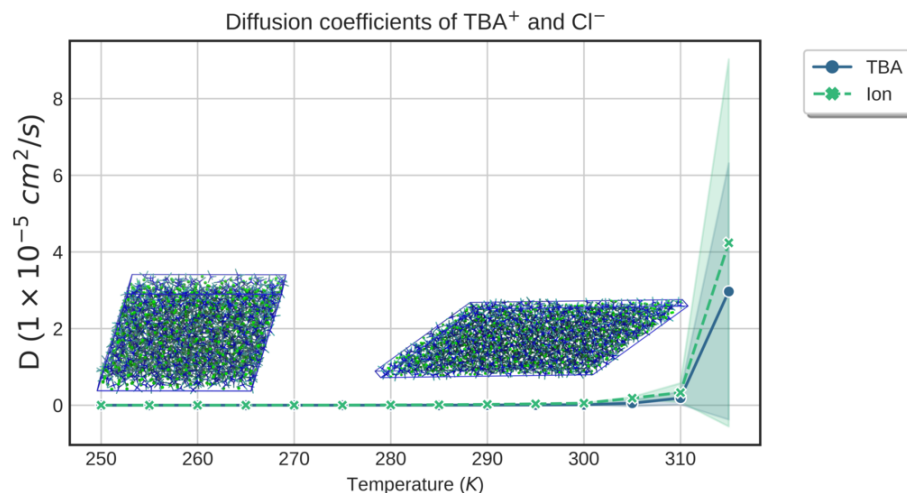


Figure 6: Melting point of crystalline TBAC. Diffusion coefficients of TBA⁺ and Cl⁻ are in blue and green, respectively. Partial melting begins at approximately 300 K, and the system reaches a fully molten state at 310 K

Applications of the DES models

2-methylthiophene and benzothiophene extraction from model fuel

The importance of cheap and effective means for desulfurization of petroleum derivatives, such as fuel, has gained well deserved attention in the recent decades due to increased awareness of the effect they have on our environment. Typical hydrodesulfurization methods are effective in the removal of aliphatic sulfur-bearing compounds, but do not fare well in removing heterocyclic organosulfuric compounds such as benzothiophene.^{100,101} ILs have been tested as potential solution to this problem,^{102,103} and this work has more recently been expanded to study whether DESs could act as solvents for extractive desulfurization of fuel.^{104–106}

In order to test the predictive capability of our DES models, we parameterized Martini 3 models for two target compounds: Benzothiophene (BTP) and 2-methylthiophene (MTP). These were solvated in octane, which has been used as a model-fuel in previous

experimental studies alongside heptane, which is almost indistinguishable from octane at the coarse-grained level. We then proceeded to extract both, MTP and BTP from the model fuel by using a TBAC - acetic acid DES in 1:2 ratio. The octane-DES mass ratio was approximately 1:1. The choice of using AcAc as a HBD, as well as the octane-DES mass ratio, were based on the experimental work of Li *et al.*, described in their 2016 study on the same topic, with the exception of using tetrabutylammonium bromide instead of TBAC.¹⁰⁶ The details of the simulation setup are given in Supplementary Information section 5. As shown in the graphical snapshot of the system (Figure 7), the octane-DES system forms a stable biphasic system starting from a homogeneously mixed initial state.

Both MTP and BTP are preferentially solvated in the DES phase, with BTP almost completely extracted, which is in line with experimental findings.¹⁰⁶ Based on 6 independent simulations, each lasting 2 μ s, we obtained a $63.2 \% \pm 5.7 \%$ extraction efficiency for MTP, and a $98.9 \% \pm 0.1 \%$ extraction efficiency for BTP. Results and a comparison to experimentally derived extraction efficiencies are given in Table 3.

We find our results in good agreement with the values reported in literature, in particular regarding the larger extraction coefficient of BTP with respect to MTP. There are a few considerations for reviewing this data: As this was just a 'proof of concept' type of test case, we did not screen various TBAC:AcAc ratios, nor DES:Oil ratios, which almost certainly would affect the extraction efficiency. In addition, we did not extract each component (MTP, BTP) individually, but at the same time. The exact method by which MTP and BTP are extracted is not fully understood. Li *et al.* propose hydrogen bonding as the primary mechanism for extraction of both BTP and thiophene,¹⁰⁰ whereas Wang *et al.* point towards CH- π interactions.¹⁰⁵

Our results suggest that the latter of the proposed mechanisms is more pronounced, since the extraction in our models is primarily driven by the favourable SC3 - TC n ($n = 2, 4, 5, 6$) interactions, which were designed to at least partially capture the CH- π interactions. In all likelihood the mechanism also relies on hydrogen bonding, which in Martini 3 is accounted

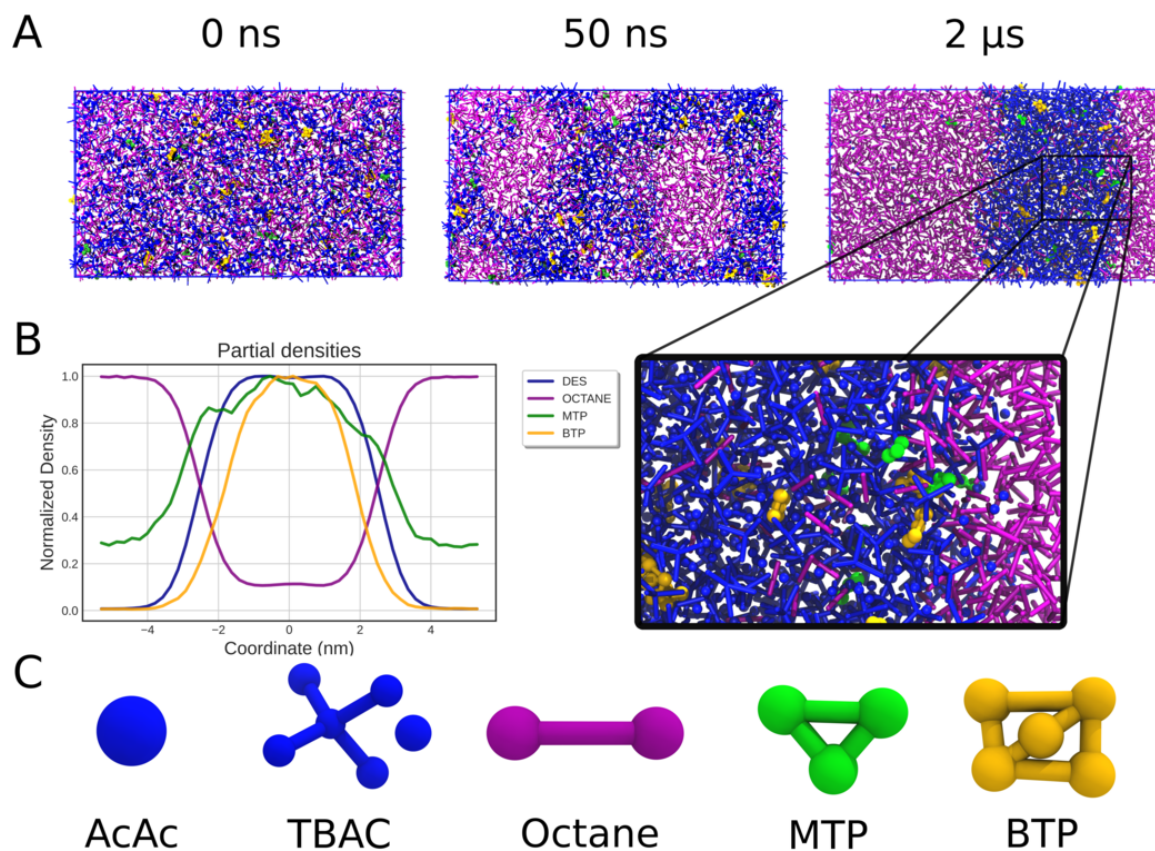


Figure 7: Extraction of MTP and BTP from octane by TBAC - AcAc DES. (A) Evolution of the DES-octane mixture over time with snapshots of the system at various times, indicating the formation of a biphasic system. (B) Partial density graph of each component, along with a zoom in to the equilibrated system. In the partial density graph MTP, line drawn in green, can be seen favouring the DES phase, but still partially residing on the interface as well as in the octane phase. BTP, drawn in yellow, is almost completely extracted. (C) Components of the simulation, with their respective colours.

for in the Lennard-Jones potential parameters.

Table 3: Extraction Efficiencies.

HBA	HBD	Solute	Fuel	Extraction efficiency (%)	Reference
TBAC	Acetic Acid	BTP	Octane	98.9 ± 0.1	This work
TBA-Br	Acetic Acid	BTP	Octane	81.75	Ref. ¹⁰⁶
TBAC	Propanoic Acid	BTP	Octane	71 - 99.47	Ref. ¹⁰⁰
TBAC	Acetic Acid	MTP	Octane	63.2 ± 5.7	This work
TBA-Br	Acetic Acid	Thiophene	Octane	55.8	Ref. ¹⁰⁶
TBAC	Malonic Acid	MTP	Octane	50.05	Ref. ¹⁰⁷

Imidacloprid extraction from water

Neonicotinoids are a class of insecticides, previously lauded for their high efficacy and low risks.¹⁰⁸ Recent discoveries have pointed towards a unwanted effects in non-target organisms, especially in pollinators,¹⁰⁹ leading to a ban in some EU-countries and in the US. Although the search for new and alternative insecticides is well on its way,¹¹⁰ neonicotinoids are still in use in many countries,¹¹¹ some of which are reporting frequent detection of neonicotinoids in drinking water.¹¹² Modern water treatment facilities use multi-step processes to remove potential unwanted residues from wastewater, but adsorption processes are still primarily used for removal of micropollutants, such as neonicotinoids.¹¹³ Typically these processes use active carbon as an adsorbent, but the successful use of ILs has also been reported in cases where more specificity is required.¹¹⁴ Development of hydrophobic DESs has sparked interest in usage of DESs in wastewater treatment, with the hopes of finding a more recyclable and cheaper alternative for ILs.

In 2017 Florindo *et al.*¹¹⁵ published their work on extracting acetamiprid, nitenpyram, thiamethoxam and imidacloprid from water using DL-menthol or TBAC based DESs. They demonstrate three successful extractions of all neonicotinoids from water with DL-menthol - carboxylic acid DESs, and report all TBAC based DESs leaching in to the water phase, contaminating it. We selected TBAC - DecA and DL-menthol - DecA as test cases, with the former reportedly failing due to TBAC leaching, and the latter being successful. For this particular test case we selected only imidacloprid (IMID) as a target. For DL-menthol - DecA systems, we set up four 2 μ s simulations. Each simulation had $\chi_{IMID}=0.01$ and 1:1 ratio between the DES components. The same was done for the TBAC - DecA systems, with the exception of 1:2 ratio between TBAC and DecA.

Our results show similar behaviour to what Florindo *et al.* have reported: TBAC-DecA DES extracts IMID, but simultaneously TBAC leaches in to the water phase. This is evident from the graphical snapshot as well as the partial density profiles, shown in Figure 8. Menthol-DecA DES extracts IMID with an average efficiency of 75.2 ± 13 %, which is some-

what higher than the experimental value, $53.06 \pm 0.23 \%$.¹¹⁵ We presume this discrepancy is partly due to the relatively high density of IMID within the interface region between the DES and water phase. The effect of the interface is much more pronounced in simulations than in experiment, due to the limited volume of our systems.

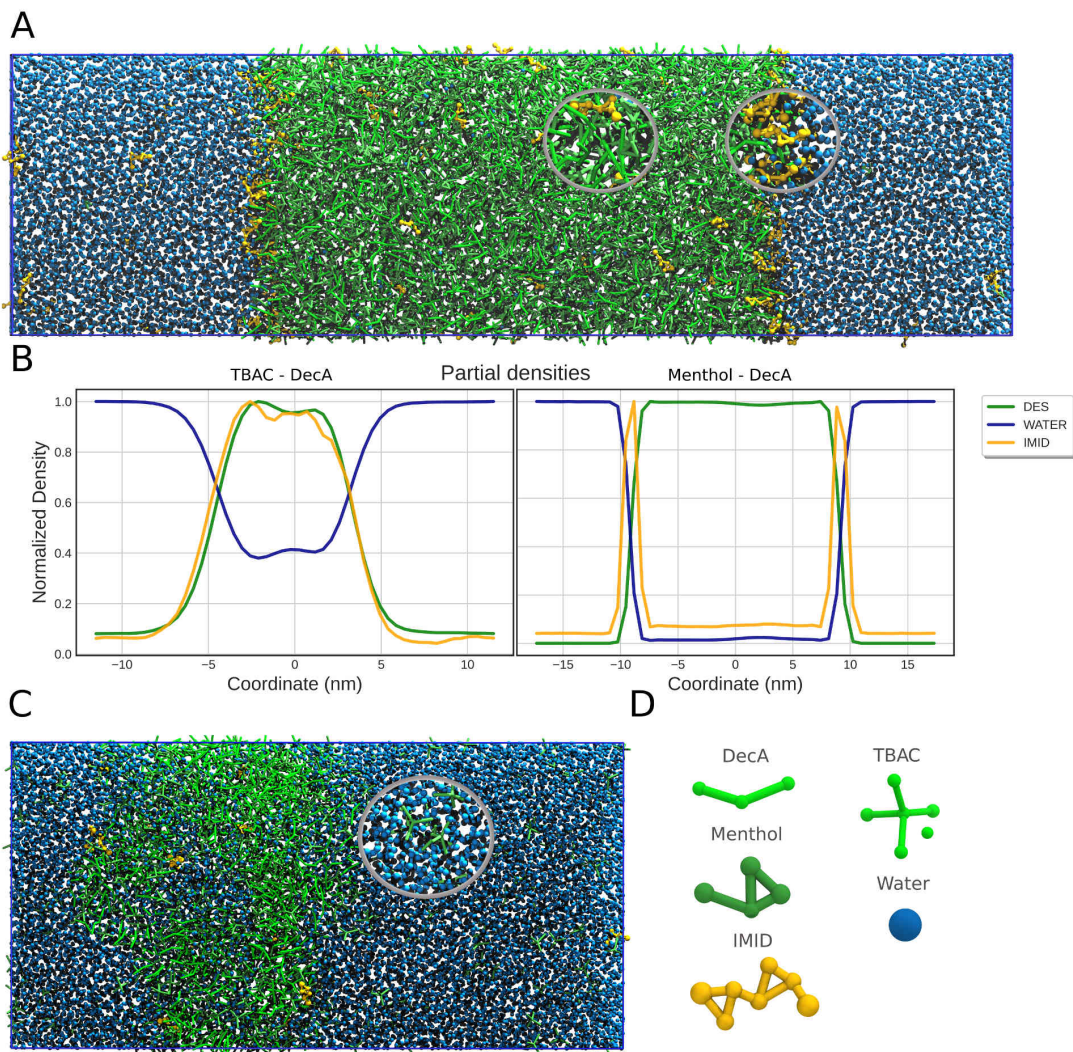


Figure 8: Extraction of IMID from water by menthol -DecA DES. (A) Menthol - DecA DES extracting IMID from water. (B) Normalized partial density profiles of systems containing TBAC - DecA (left) or menthol - DecA (right). (C) TBAC - DecA DES in water, with TBA⁺ leaching to the aqueous phase. (D) Compounds present in the simulation, with their corresponding colours.

The accumulation of IMID at the interface is remarkable. Separate simulations of IMID in pure DES show ready solubility of IMID in menthol - DecA; even at mole fractions as high

as $\chi_{IMID} = 0.12$ IMID remains soluble. Without further validation and experimental data, it is impossible to say whether or not the enrichment at the interface is an artefact of the simulation, or realistic. However, the relatively well matching extraction efficiency and high solubility of IMID in pure DES point towards the latter option. Florindo *et al.* concluded that the main driving force for the extraction was the hydrophobicity of the neonicotinoid solute, but called for further investigation. The behaviour of IMID observed in our simulations is in line with this conclusion, and further observations can be made: At the interface we observe a significant percentage of IMID aligned with the more hydrophobic chloropyridine moiety facing the DES phase, and the nitramide-like moiety facing the aqueous phase. As IMID diffuses along the interface and changes its orientation, an attractive interaction between the nitramide-moiety of IMID and the carboxylic acid group of DecA (or the hydroxyl group in menthol) comes into play, stabilizing the extraction of IMID to the DES phase.

Surfactant self-assembly in choline chloride - urea DES

Arnold *et al.* reported sodium dodecyl sulfate (SDS) forming larger self-assembled structures when immersed in choline chloride - urea DES.¹¹⁶ SDS typically forms spherical micelles when immersed in water, but Arnold *et al.* observed cylinder-like formations, and surface activity below the critical micelle concentration (CMC). They reported, among other things, the length and radii of these formations as a function of mole fraction of SDS, presenting us a prime opportunity to test our models.

We set up simulations using six equally spaced mole fractions for SDS, ranging from $\chi_{SDS} = 0.0025$ to $\chi_{SDS} = 0.015$, randomly placing them in a 1:2-ratio choline chloride - urea DES. Each simulation lasted 3 μ s. Reference simulations were performed, in which same amounts of SDS were solvated in water for an equal time. For each system, we computed the length of the micelle, the radius of gyration and moments of inertia, and asphericity. We also report the number of micelles present in the system in the last 1 μ s of the simulation. All numerical data is reported in the Supplementary Information section 9. The results show

that our models reproduce the phenomenon reported by Arnold *et al.*: The formation of cylinder-like SDS micelles in the DES, and spherical SDS micelles in water. The behaviour in water and DES is illustrated in Figure 9. As a final test, one of the elongated micelles was removed from the DES phase and solvated with water in order to study whether it would remain stable in the aqueous phase. As is evident from the inset in Figure 9, the micelle rapidly disintegrates and begins to form spherical micelles.

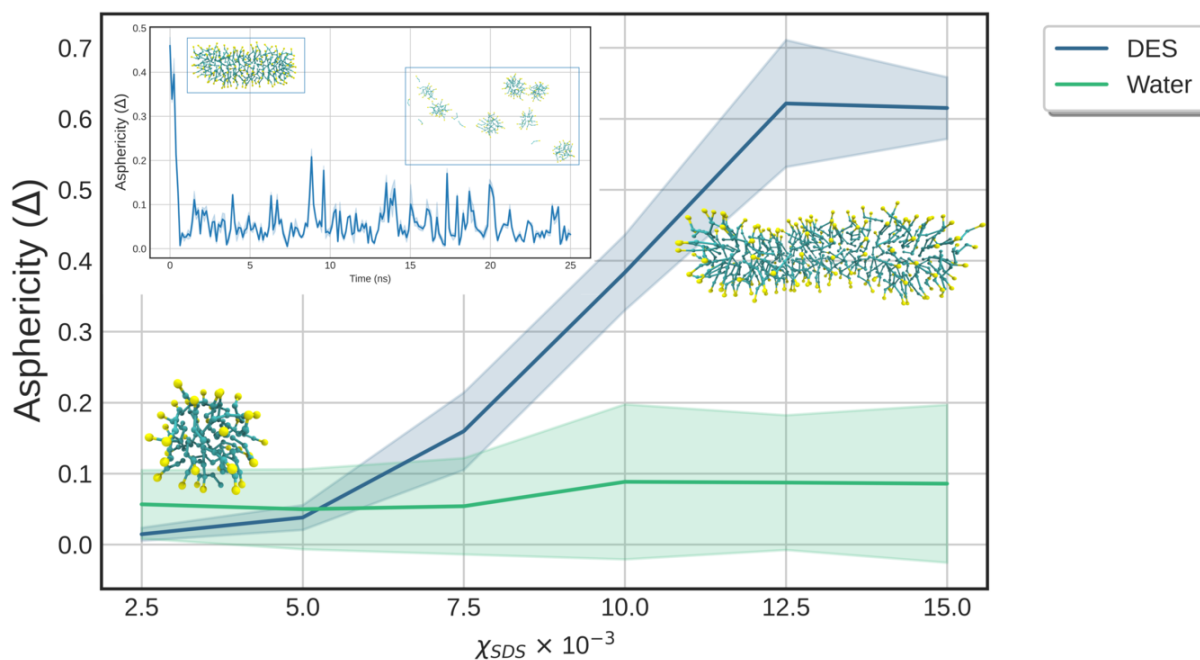


Figure 9: Asphericity of SDS micelles as a function of the mole fraction of SDS in DES. Corresponding values for water are given in the Supplementary Information section 9. Inset: An elongated micelle breaking to multiple spherical micelles when removed from the DES and solvated with water.

It is not entirely clear what drives this behaviour. A more recent publication on the topic proposed that the elongation is due to counterion condensation, which implies that the Stern layer around the micelle should be primarily occupied by sodium when immersed in DES. This will, in turn, reduce the repulsion between the dodecyl sulfate headgroups, allowing for elongation.¹¹⁷ Our models reproduce this, with the exception of the Stern layer being primarily occupied by the choline-cations instead of sodium. Another contradiction

is observed when the micelle is solvated in water. Our models indicate that the sodium cations prefer binding to the micelle headgroup instead of residing in the aqueous phase. This finding is supported by computational work done by Tang *et al.*,¹¹⁸ who report that the bulk of the sodium is residing within 6 Å of the micelle when solvated in water.

Taken together, our results point to a replacement of sodium by choline cations when the micelles are solvated in choline chloride - urea DES. Given the much higher concentration of choline cations inside the DES with respect to sodium ions in the aqueous phase, the interactions between the charged SDS headgroups are much better screened, changing the effective curvature of the molecules toward less positive values and driving the transition to a less curved assembly.

Conclusions

We propose the first CG models for type III DESs and NADESs. Our models are capable of reproducing density, liquid structure and thermal expansion coefficients of pure DESs with relatively good agreement with experiment. We demonstrated the transferability of our models with three varied test cases, all of which were in good agreement with experiment. Compared to the existing atomistic force fields, our approach offers some important advantages: Coarse-graining allows for larger system sizes and longer simulations, reducing the need to use HPC facilities, and enables the study of more complex systems and processes, such as LLE, on more reasonable timescales. Furthermore, since the DES models are parameterized for Martini 3, following the same parameterization strategy, they are compatible with other Martini 3 models, and can be used in combination with biomolecular or polymeric systems. The availability of more systematic experimental data, in particular on partitioning of compounds between DESs and other solvents would facilitate the extension of our current DES topologies using the approach described in the paper.

As the library of validated DES compounds grows, Martini based simulations can be

used for high throughput studies of existing DESs, and potentially for virtual screening of new DESs more suitable for selective extractions.

Supporting Information Available

Model data and parameters, comparison of bonded terms, SASA numerical data, TI routine, system compositions, densities, SDS micelle numerical data, viscosity data.

Acknowledgement

PAV would like to thank R. Alessandri, F. Grünewald and A.H. de Vries for many helpful discussions. The MD simulations were carried out on the Dutch national e-infrastructure with the support of SURFsara.

References

- (1) Abbott, A. P.; Al-Barzinjy, A. A.; Abbott, P. D.; Frisch, G.; Harris, R. C.; Hartley, J.; Ryder, K. S. Speciation, physical and electrolytic properties of eutectic mixtures based on $\text{CrCl}_3 \cdot 6\text{H}_2\text{O}$ and urea. *Phys. Chem. Chem. Phys.* **2014**, *16*, 9047–9055.
- (2) Smith, E. L.; Abbott, A. P.; Ryder, K. S. Deep Eutectic Solvents (DESs) and Their Applications. *Chemical Reviews* **2014**, *114*, 11060–11082, PMID: 25300631.
- (3) Martins, M. A. R.; Pinho, S. P.; Coutinho, J. A. P. Insights into the Nature of Eutectic and Deep Eutectic Mixtures. *Journal of Solution Chemistry* **2019**, *48*, 962–982.
- (4) Choi, Y. H.; van Spronsen, J.; Dai, Y.; Verberne, M.; Hollmann, F.; Arends, I. W.; Witkamp, G.-J.; Verpoorte, R. Are Natural Deep Eutectic Solvents the Missing Link in Understanding Cellular Metabolism and Physiology? *Plant Physiology* **2011**, *156*, 1701–1705.

- (5) Zhekenov, T.; Toksanbayev, N.; Kazakbayeva, Z.; Shah, D.; Mjalli, F. S. Formation of type III Deep Eutectic Solvents and effect of water on their intermolecular interactions. *Fluid Phase Equilibria* **2017**, *441*, 43–48, 2016 Asian Thermophysical Properties Conference.
- (6) Paiva, A.; Matias, A. A.; Duarte, A. R. C. How do we drive deep eutectic systems towards an industrial reality? *Current Opinion in Green and Sustainable Chemistry* **2018**, *11*, 81–85, Pharmaceuticals / Green Processes and Technologies.
- (7) Gill, I.; Vulfson, E. Enzymic catalysis in heterogeneous eutectic mixtures of substrates. *Trends in Biotechnology* **1994**, *12*, 118–122.
- (8) Lopez-Fandino, R.; Gill, I.; Vulfson, E. N. Protease-catalyzed synthesis of oligopeptides in heterogenous substrate mixtures. *Biotechnology and Bioengineering* **1994**, *43*, 1024–1030.
- (9) Abbott, A. P.; Capper, G.; Davies, D. L.; Rasheed, R. K.; Tambyrajah, V. Novel solvent properties of choline chloride/urea mixtures. *Chem. Commun.* **2003**, 70–71.
- (10) Abbott, A. P.; Boothby, D.; Capper, G.; Davies, D. L.; Rasheed, R. K. Deep Eutectic Solvents Formed between Choline Chloride and Carboxylic Acids: Versatile Alternatives to Ionic Liquids. *Journal of the American Chemical Society* **2004**, *126*, 9142–9147, PMID: 15264850.
- (11) Dai, Y.; Witkamp, G.-J.; Verpoorte, R.; Choi, Y. H. Tailoring properties of natural deep eutectic solvents with water to facilitate their applications. *Food Chemistry* **2015**, *187*, 14–19.
- (12) Abo-Hamad, A.; Hayyan, M.; Saadi, M. A. H. A.; Hashim, M. A. Potential applications of deep eutectic solvents in nanotechnology. *Chemical Engineering Journal* **2015**, *273*, 551–567.

- (13) Zhang, Q.; De Oliveira Vigier, K.; Royer, S.; Jérôme, F. Deep eutectic solvents: syntheses, properties and applications. *Chem. Soc. Rev.* **2012**, *41*, 7108–7146.
- (14) Carriazo, D.; Serrano, M. C.; Gutiérrez, M. C.; Ferrer, M. L.; del Monte, F. Deep eutectic solvents playing multiple roles in the synthesis of polymers and related materials. *Chem. Soc. Rev.* **2012**, *41*, 4996–5014.
- (15) Perna, F. M.; Vitale, P.; Capriati, V. Deep eutectic solvents and their applications as green solvents. *Current Opinion in Green and Sustainable Chemistry* **2020**, *21*, 27–33, New Synthetic methods Selected papers from the 4th Green and Sustainable Chemistry Conference.
- (16) Xu, G.-C.; Ding, J.-C.; Han, R.-Z.; Dong, J.-J.; Ni, Y. Enhancing cellulose accessibility of corn stover by deep eutectic solvent pretreatment for butanol fermentation. *Bioresource Technology* **2016**, *203*, 364–369.
- (17) Lapena, D.; Errazquin, D.; Lomba, L.; Lafuente, C.; Beatriz, G. Ecotoxicity and biodegradability of pure and aqueous mixtures of deep eutectic solvents: glyceline, ethaline, and reline. *Environmental Science and Pollution Research* **2021**, *28*, 8812–8821.
- (18) Li, P.; Sirviö, J. A.; Asante, B.; Liimatainen, H. Recyclable deep eutectic solvent for the production of cationic nanocelluloses. *Carbohydrate Polymers* **2018**, *199*, 219–227.
- (19) Haghbakhsh, R.; Raeissi, S.; Duarte, A. R. C. Group contribution and atomic contribution models for the prediction of various physical properties of deep eutectic solvents. *Scientific Reports* **2021**, *11*, 6684.
- (20) Alkhatib, I. I.; Bahamon, D.; Llovel, F.; Abu-Zahra, M. R.; Vega, L. F. Perspectives and guidelines on thermodynamic modelling of deep eutectic solvents. *Journal of Molecular Liquids* **2020**, *298*, 112183.

- (21) Kaur, S.; Malik, A.; Kashyap, H. K. Anatomy of Microscopic Structure of Ethaline Deep Eutectic Solvent Decoded through Molecular Dynamics Simulations. *The Journal of Physical Chemistry B* **2019**, *123*, 8291–8299, PMID: 31448914.
- (22) Kumari, P.; Shobhna,; Kaur, S.; Kashyap, H. K. Influence of Hydration on the Structure of Reline Deep Eutectic Solvent: A Molecular Dynamics Study. *ACS Omega* **2018**, *3*, 15246–15255.
- (23) Atilhan, M.; Aparicio, S. Molecular dynamics simulations of mixed deep eutectic solvents and their interaction with nanomaterials. *Journal of Molecular Liquids* **2019**, *283*, 147–154.
- (24) Triolo, A.; Celso, F. L.; Brehm, M.; Lisio, V. D.; Russina, O. Liquid structure of a choline chloride-water natural deep eutectic solvent: A molecular dynamics characterization. *Journal of Molecular Liquids* **2021**, *331*, 115750.
- (25) Salehi, H. S.; Ramdin, M.; Moulton, O. A.; Vlugt, T. J. Computing solubility parameters of deep eutectic solvents from Molecular Dynamics simulations. *Fluid Phase Equilibria* **2019**, *497*, 10–18.
- (26) Kaur, S.; Kumari, M.; Kashyap, H. K. Microstructure of Deep Eutectic Solvents: Current Understanding and Challenges. *The Journal of Physical Chemistry B* **2020**, *124*, 10601–10616, PMID: 33151072.
- (27) Shahbaz, K.; Mjalli, F.; Hashim, M.; AlNashef, I. Prediction of deep eutectic solvents densities at different temperatures. *Thermochimica Acta* **2011**, *515*, 67–72.
- (28) Adeyemi, I.; Abu-Zahra, M. R.; AlNashef, I. M. Physicochemical properties of alkanolamine-choline chloride deep eutectic solvents: Measurements, group contribution and artificial intelligence prediction techniques. *Journal of Molecular Liquids* **2018**, *256*, 581–590.

- (29) Bezold, F.; Weinberger, M. E.; Minceva, M. Assessing solute partitioning in deep eutectic solvent-based biphasic systems using the predictive thermodynamic model COSMO-RS. *Fluid Phase Equilibria* **2017**, *437*, 23–33.
- (30) Liu, Y.; Yu, H.; Sun, Y.; Zeng, S.; Zhang, X.; Nie, Y.; Zhang, S.; Ji, X. Screening Deep Eutectic Solvents for CO₂ Capture With COSMO-RS. *Frontiers in Chemistry* **2020**, *8*, 82.
- (31) Abranches, D. O.; Larriba, M.; Silva, L. P.; Melle-Franco, M.; Palomar, J. F.; Pinho, S. P.; Coutinho, J. A. Using COSMO-RS to design choline chloride pharmaceutical eutectic solvents. *Fluid Phase Equilibria* **2019**, *497*, 71–78.
- (32) Gutiérrez, A.; Atilhan, M.; Aparicio, S. Theoretical Study on Deep Eutectic Solvents as Vehicles for the Delivery of Anesthetics. *The Journal of Physical Chemistry B* **2020**, *124*, 1794–1805, PMID: 32049519.
- (33) González de Castilla, A.; Bittner, J. P.; Müller, S.; Jakobtorweihen, S.; Smirnova, I. Thermodynamic and Transport Properties Modeling of Deep Eutectic Solvents: A Review on gE-Models, Equations of State, and Molecular Dynamics. *Journal of Chemical & Engineering Data* **2020**, *65*, 943–967.
- (34) Merchant, B. A.; Madura, J. D. In *Annual Reports in Computational Chemistry*; Wheeler, R. A., Ed.; Annual Reports in Computational Chemistry; Elsevier, 2011; Vol. 7; pp 67–87.
- (35) Joshi, S. Y.; Deshmukh, S. A. A review of advancements in coarse-grained molecular dynamics simulations. *Molecular Simulation* **2020**, *0*, 1–18.
- (36) Ingólfsson, H. I.; Lopez, C. A.; Uusitalo, J. J.; de Jong, D. H.; Gopal, S. M.; Periole, X.; Marrink, S. J. The power of coarse graining in biomolecular simulations. *WIREs Computational Molecular Science* **2014**, *4*, 225–248.

- (37) Marrink, S. J.; Risselada, H. J.; Yefimov, S.; Tieleman, D. P.; de Vries, A. H. The MARTINI Force Field: Coarse Grained Model for Biomolecular Simulations. *The Journal of Physical Chemistry B* **2007**, *111*, 7812–7824, PMID: 17569554.
- (38) Melo, M. N.; Arnarez, C.; Sikkema, H.; Kumar, N.; Walko, M.; Berendsen, H. J. C.; Kocer, A.; Marrink, S. J.; Ingólfsson, H. I. High-Throughput Simulations Reveal Membrane-Mediated Effects of Alcohols on MscL Gating. *Journal of the American Chemical Society* **2017**, *139*, 2664–2671, PMID: 28122455.
- (39) Moiset, G.; López, C. A.; Bartelds, R.; Syga, L.; Rijpkema, E.; Cukkemane, A.; Balduş, M.; Poolman, B.; Marrink, S. J. Disaccharides Impact the Lateral Organization of Lipid Membranes. *Journal of the American Chemical Society* **2014**, *136*, 16167–16175, PMID: 25316578.
- (40) Ingólfsson, H. I.; Melo, M. N.; van Eerden, F. J.; Arnarez, C.; Lopez, C. A.; Wassenaar, T. A.; Periolo, X.; de Vries, A. H.; Tieleman, D. P.; Marrink, S. J. Lipid Organization of the Plasma Membrane. *Journal of the American Chemical Society* **2014**, *136*, 14554–14559, PMID: 25229711.
- (41) Souza, P. C. T.; Thallmair, S.; Conflitti, P.; Ramirez-Palacios, C.; Alessandri, R.; Raniolo, S.; Limongelli, V.; Marrink, S. J. Protein–ligand binding with the coarse-grained Martini model. *Nature Communications* **2020**, *11*, 3714.
- (42) Dadsena, S.; Bockelmann, S.; Mina, J. G. M.; Hassan, D. G.; Korneev, S.; Razzera, G.; Jahn, H.; Niekamp, P.; Muller, D.; Schneider, M.; Tafesse, F. G.; Marrink, S. J.; Melo, M. N.; Holthuis, J. C. M. Ceramides bind VDAC2 to trigger mitochondrial apoptosis. *Nature Communications* **2019**, *10*, 1832.
- (43) Vazquez-Salazar, L. I.; Selle, M.; de Vries, A. H.; Marrink, S. J.; Souza, P. C. T. Martini coarse-grained models of imidazolium-based ionic liquids: from nanostructural organization to liquid–liquid extraction. *Green Chem.* **2020**, *22*, 7376–7386.

- (44) Alessandri, R.; Sami, S.; Barnoud, J.; de Vries, A. H.; Marrink, S. J.; Havenith, R. W. A. Resolving Donor–Acceptor Interfaces and Charge Carrier Energy Levels of Organic Semiconductors with Polar Side Chains. *Advanced Functional Materials* **2020**, *30*, 2004799.
- (45) Piskorz, T. K.; Gobbo, C.; Marrink, S. J.; De Feyter, S.; de Vries, A. H.; van Esch, J. H. Nucleation Mechanisms of Self-Assembled Physisorbed Monolayers on Graphite. *The Journal of Physical Chemistry C* **2019**, *123*, 17510–17520.
- (46) Alessandri, R.; Uusitalo, J. J.; de Vries, A. H.; Havenith, R. W. A.; Marrink, S. J. Bulk Heterojunction Morphologies with Atomistic Resolution from Coarse-Grain Solvent Evaporation Simulations. *Journal of the American Chemical Society* **2017**, *139*, 3697–3705, PMID: 28209056.
- (47) Souza, P. C. T. et al. Martini 3: a general purpose force field for coarse-grained molecular dynamics. *Nature Methods* **2021**, *18*, 382–388.
- (48) Abraham, M. J.; Murtola, T.; Schulz, R.; Páll, S.; Smith, J. C.; Hess, B.; Lindahl, E. GROMACS: High performance molecular simulations through multi-level parallelism from laptops to supercomputers. *SoftwareX* **2015**, *1-2*, 19–25.
- (49) Páll, S.; Abraham, M. J.; Kutzner, C.; Hess, B.; Lindahl, E. Tackling Exascale Software Challenges in Molecular Dynamics Simulations with GROMACS. Solving Software Challenges for Exascale. Cham, 2015; pp 3–27.
- (50) Pronk, S.; Páll, S.; Schulz, R.; Larsson, P.; Bjelkmar, P.; Apostolov, R.; Shirts, M. R.; Smith, J. C.; Kasson, P. M.; van der Spoel, D.; Hess, B.; Lindahl, E. GROMACS 4.5: a high-throughput and highly parallel open source molecular simulation toolkit. *Bioinformatics* **2013**, *29*, 845–854.
- (51) Hess, B.; Kutzner, C.; van der Spoel, D.; Lindahl, E. GROMACS 4: Algorithms

- for Highly Efficient, Load-Balanced, and Scalable Molecular Simulation. *Journal of Chemical Theory and Computation* **2008**, *4*, 435–447, PMID: 26620784.
- (52) Van Der Spoel, D.; Lindahl, E.; Hess, B.; Groenhof, G.; Mark, A. E.; Berendsen, H. J. C. GROMACS: Fast, flexible, and free. *Journal of Computational Chemistry* **2005**, *26*, 1701–1718.
- (53) Lindahl, E.; Hess, B.; van der Spoel, D. GROMACS 3.0: a package for molecular simulation and trajectory analysis. *Molecular modeling annual* **2001**, *7*, 306–317.
- (54) Berendsen, H.; van der Spoel, D.; van Drunen, R. GROMACS: A message-passing parallel molecular dynamics implementation. *Computer Physics Communications* **1995**, *91*, 43–56.
- (55) Bussi, G.; Donadio, D.; Parrinello, M. Canonical sampling through velocity rescaling. *The Journal of Chemical Physics* **2007**, *126*, 014101.
- (56) Berendsen, H. J. C.; Postma, J. P. M.; van Gunsteren, W. F.; DiNola, A.; Haak, J. R. Molecular dynamics with coupling to an external bath. *The Journal of Chemical Physics* **1984**, *81*, 3684–3690.
- (57) Parrinello, M.; Rahman, A. Polymorphic transitions in single crystals: A new molecular dynamics method. *Journal of Applied Physics* **1981**, *52*, 7182–7190.
- (58) Hess, B. P-LINCS: A Parallel Linear Constraint Solver for Molecular Simulation. *Journal of Chemical Theory and Computation* **2008**, *4*, 116–122, PMID: 26619985.
- (59) Essmann, U.; Perera, L.; Berkowitz, M. L.; Darden, T.; Lee, H.; Pedersen, L. G. A smooth particle mesh Ewald method. *The Journal of Chemical Physics* **1995**, *103*, 8577–8593.

- (60) Huang, J.; Rauscher, S.; Nawrocki, G.; Ran, T.; Feig, M.; de Groot, B. L.; Grubmuller, H.; MacKerell, A. D. CHARMM36m: an improved force field for folded and intrinsically disordered proteins. *Nature Methods* **2017**, *14*, 71–73.
- (61) Best, R. B.; Zhu, X.; Shim, J.; Lopes, P. E. M.; Mittal, J.; Feig, M.; MacKerell, A. D. Optimization of the Additive CHARMM All-Atom Protein Force Field Targeting Improved Sampling of the Backbone ϕ and Side-Chain χ_1 and χ_2 Dihedral Angles. *Journal of Chemical Theory and Computation* **2012**, *8*, 3257–3273, PMID: 23341755.
- (62) Bjelkmar, P.; Larsson, P.; Cuendet, M. A.; Hess, B.; Lindahl, E. Implementation of the CHARMM Force Field in GROMACS: Analysis of Protein Stability Effects from Correction Maps, Virtual Interaction Sites, and Water Models. *Journal of Chemical Theory and Computation* **2010**, *6*, 459–466, PMID: 26617301.
- (63) Macrae, C. F.; Sovago, I.; Cottrell, S. J.; Galek, P. T. A.; McCabe, P.; Pidcock, E.; Platings, M.; Shields, G. P.; Stevens, J. S.; Towler, M.; Wood, P. A. *Mercury 4.0*: from visualization to analysis, design and prediction. *Journal of Applied Crystallography* **2020**, *53*, 226–235.
- (64) Macrae, C. F.; Bruno, I. J.; Chisholm, J. A.; Edgington, P. R.; McCabe, P.; Pidcock, E.; Rodriguez-Monge, L.; Taylor, R.; van de Streek, J.; Wood, P. A. *Mercury CSD 2.0* – new features for the visualization and investigation of crystal structures. *Journal of Applied Crystallography* **2008**, *41*, 466–470.
- (65) Macrae, C. F.; Edgington, P. R.; McCabe, P.; Pidcock, E.; Shields, G. P.; Taylor, R.; Towler, M.; van de Streek, J. *Mercury*: visualization and analysis of crystal structures. *Journal of Applied Crystallography* **2006**, *39*, 453–457.
- (66) Bruno, I. J.; Cole, J. C.; Edgington, P. R.; Kessler, M.; Macrae, C. F.; McCabe, P.; Pearson, J.; Taylor, R. New software for searching the Cambridge Structural Database and visualizing crystal structures. *Acta Crystallographica Section B* **2002**, *58*, 389–397.

- (67) Taylor, R.; Macrae, C. F. Rules governing the crystal packing of mono- and dialcohols. *Acta Crystallographica Section B* **2001**, *57*, 815–827.
- (68) Graham, J. A.; Essex, J. W.; Khalid, S. PyCGTOOL: Automated Generation of Coarse-Grained Molecular Dynamics Models from Atomistic Trajectories. *Journal of Chemical Information and Modeling* **2017**, *57*, 650–656.
- (69) Souza, P. C. T.; Marrink, S. J. Martini 3 - Open Beta-Release. 2020; <http://cgmartini.nl>.
- (70) Alessandri, R.; Barnoud, J.; Gertsen, A. S.; Patmanidis, I.; de Vries, A. H.; Souza, P. C. T.; Marrink, S. J. Martini 3 Coarse-Grained Force Field: Small Molecules. *ChemRxiv* **2021**,
- (71) Zoete, V.; Cuendet, M. A.; Grosdidier, A.; Michielin, O. SwissParam: A fast force field generation tool for small organic molecules. *Journal of Computational Chemistry* **2011**, *32*, 2359–2368.
- (72) Sami, S. Organic Materials in Silico: From force field development to predicting dielectric properties. Ph.D. thesis, University of Groningen, 2020.
- (73) Bondi, A. van der Waals Volumes and Radii. *The Journal of Physical Chemistry* **1964**, *68*, 441–451.
- (74) Rowland, R. S.; Taylor, R. Intermolecular Nonbonded Contact Distances in Organic Crystal Structures: Comparison with Distances Expected from van der Waals Radii. *The Journal of Physical Chemistry* **1996**, *100*, 7384–7391.
- (75) Breneman, C. M.; Wiberg, K. B. Determining atom-centered monopoles from molecular electrostatic potentials. The need for high sampling density in formamide conformational analysis. *Journal of Computational Chemistry* **1990**, *11*, 361–373.
- (76) Frisch, M. J. et al. Gaussian~16 Revision C.01. 2016; Gaussian Inc. Wallingford CT.

- (77) Dima, R. I.; Thirumalai, D. Asymmetry in the Shapes of Folded and Denatured States of Proteins. *The Journal of Physical Chemistry B* **2004**, *108*, 6564–6570.
- (78) Gowers, R. J.; Linke, M.; Barnoud, J.; Reddy, T. J. E.; Melo, M. N.; Seyler, S. L.; Domański, J.; Dotson, D. L.; Buchoux, S.; Kenney, I. M.; Beckstein, O. MDAnalysis: A Python Package for the Rapid Analysis of Molecular Dynamics Simulations. Proceedings of the 15th Python in Science Conference. 2016; pp 98–105.
- (79) Michaud-Agrawal, N.; Denning, E. J.; Woolf, T. B.; Beckstein, O. MDAnalysis: A toolkit for the analysis of molecular dynamics simulations. *Journal of Computational Chemistry* **2011**, *32*, 2319–2327.
- (80) Maginn, E. J.; Messerly, R. A.; Carlson, D. J.; Roe, D. R.; Elliot, J. R. Best Practices for Computing Transport Properties 1. Self-Diffusivity and Viscosity from Equilibrium Molecular Dynamics [Article v1.0]. *Living Journal of Computational Molecular Science* **2018**, *1*, 6324.
- (81) Kivelä, H.; Salomäki, M.; Vainikka, P.; Mäkilä, E.; Poletti, F.; Ruggeri, S.; Terzi, F.; Lukkari, J. The Effect of Water on a Hydrophobic Deep Eutectic Solvent. *Manuscript in submission*. **2021**,
- (82) Zubeir, L. F.; van Osch, D. J. G. P.; Rocha, M. A. A.; Banat, F.; Kroon, M. C. Carbon Dioxide Solubilities in Decanoic Acid-Based Hydrophobic Deep Eutectic Solvents. *Journal of Chemical & Engineering Data* **2018**, *63*, 913–919.
- (83) Lemaoui, T.; Darwish, A. S.; Attoui, A.; Abu Hatab, F.; Hammoudi, N. E. H.; Benguerba, Y.; Vega, L. F.; Alnashef, I. M. Predicting the density and viscosity of hydrophobic eutectic solvents: towards the development of sustainable solvents. *Green Chem.* **2020**, *22*, 8511–8530.
- (84) Leron, R. B.; Li, M.-H. High-pressure density measurements for choline chloride: Urea

- deep eutectic solvent and its aqueous mixtures at $T=(298.15 \text{ to } 323.15)\text{K}$ and up to 50MPa. *The Journal of Chemical Thermodynamics* **2012**, *54*, 293–301.
- (85) Yadav, A.; Pandey, S. Densities and Viscosities of (Choline Chloride + Urea) Deep Eutectic Solvent and Its Aqueous Mixtures in the Temperature Range 293.15 K to 363.15 K. *Journal of Chemical & Engineering Data* **2014**, *59*, 2221–2229.
- (86) Xie, Y.; Dong, H.; Zhang, S.; Lu, X.; Ji, X. Effect of Water on the Density, Viscosity, and CO₂ Solubility in Choline Chloride/Urea. *Journal of Chemical & Engineering Data* **2014**, *59*, 3344–3352.
- (87) van Osch, D. J.; Zubeir, L. F.; van den Bruinhorst, A.; Rocha, M. A.; Kroon, M. C. Hydrophobic deep eutectic solvents as water-immiscible extractants. *Green Chem.* **2015**, *17*, 4518–4521.
- (88) Martins, M. A. R.; Crespo, E. A.; Pontes, P. V. A.; Silva, L. P.; Bülow, M.; Maximo, G. J.; Batista, E. A. C.; Held, C.; Pinho, S. P.; Coutinho, J. A. P. Tunable Hydrophobic Eutectic Solvents Based on Terpenes and Monocarboxylic Acids. *ACS Sustainable Chemistry & Engineering* **2018**, *6*, 8836–8846.
- (89) D’Agostino, C.; Harris, R. C.; Abbott, A. P.; Gladden, L. F.; Mantle, M. D. Molecular motion and ion diffusion in choline chloride based deep eutectic solvents studied by ¹H pulsed field gradient NMR spectroscopy. *Phys. Chem. Chem. Phys.* **2011**, *13*, 21383–21391.
- (90) Omar, K. A.; Sadeghi, R. Novel Nonanol-Based deep eutectic solvents: Thermophysical properties and their applications in Liquid-Liquid extraction and amino acid detection. *Journal of Molecular Liquids* **2021**, *336*, 116359.
- (91) Al-Akayleh, F.; Mohammed Ali, H. H.; Ghareeb, M. M.; Al-Remawi, M. Therapeutic deep eutectic system of capric acid and menthol: Characterization and pharmaceutical application. *Journal of Drug Delivery Science and Technology* **2019**, *53*, 101159.

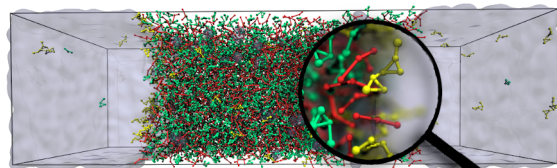
- (92) Putz, M. V. *QSAR and Spectral-SAR in Computational Ecotoxicology (1st ed.)*; CRC Press, 2012; p 242.
- (93) Klopman, G.; Li, J.-Y.; Wang, S.; Dimayuga, M. Computer Automated log P Calculations Based on an Extended Group Contribution Approach. *Journal of Chemical Information and Computer Sciences* **1994**, *34*, 752–781.
- (94) Hansch, C.; Dunn, W. J. Linear Relationships between Lipophilic Character and Biological Activity of Drugs. *Journal of Pharmaceutical Sciences* **1972**, *61*, 1–19.
- (95) Lewis, K. A.; Tzilivakis, J.; Warner, D. J.; Green, A. An international database for pesticide risk assessments and management. *Human and Ecological Risk Assessment: An International Journal* **2016**, *22*, 1050–1064.
- (96) Cornford, E. M. Correlation between lipid partition coefficients and surface permeation in *Schistosoma japonicum*. *The Journal of Membrane Biology* **1982**, *64*, 217–224.
- (97) Montgomery, J.; Crompton, T. *Environmental Chemicals Desk Reference*; CRC Press, 2017; p 1691.
- (98) Kidd, H.; James, D.; of Chemistry. Information Services., R. S. *The agrochemicals handbook*, 3rd ed.; The Royal Society of Chemistry: Cambridge, 1991; p 1200.
- (99) Coker, T. G.; Ambrose, J.; Janz, G. J. Fusion properties of some ionic quaternary ammonium compounds. *Journal of the American Chemical Society* **1970**, *92*, 5293–5297.
- (100) Li, C.; Li, D.; Zou, S.; Li, Z.; Yin, J.; Wang, A.; Cui, Y.; Yao, Z.; Zhao, Q. Extraction desulfurization process of fuels with ammonium-based deep eutectic solvents. *Green Chem.* **2013**, *15*, 2793–2799.

- (101) Girgis, M. J.; Gates, B. C. Reactivities, reaction networks, and kinetics in high-pressure catalytic hydroprocessing. *Industrial & Engineering Chemistry Research* **1991**, *30*, 2021–2058.
- (102) Asumana, C.; Yu, G.; Li, X.; Zhao, J.; Liu, G.; Chen, X. Extractive desulfurization of fuel oils with low-viscosity dicyanamide-based ionic liquids. *Green Chem.* **2010**, *12*, 2030–2037.
- (103) Syntyhaki, E.; Karonis, D. Oxidative and extractive desulfurization of petroleum middle distillates, using imidazole ionic liquids. *Fuel Communications* **2021**, *7*, 100011.
- (104) Tang, X.-d.; Zhang, Y.-f.; Li, J.-j.; Zhu, Y.-q.; Qing, D.-y.; Deng, Y.-x. Deep Extractive Desulfurization with Arenium Ion Deep Eutectic Solvents. *Industrial & Engineering Chemistry Research* **2015**, *54*, 4625–4632.
- (105) Wang, X.; Jiang, W.; Zhu, W.; Li, H.; Yin, S.; Chang, Y.; Li, H. A simple and cost-effective extractive desulfurization process with novel deep eutectic solvents. *RSC Adv.* **2016**, *6*, 30345–30352.
- (106) Li, J.-j.; Xiao, H.; Tang, X.-d.; Zhou, M. Green Carboxylic Acid-Based Deep Eutectic Solvents as Solvents for Extractive Desulfurization. *Energy & Fuels* **2016**, *30*, 5411–5418.
- (107) Shu, C.; Sun, T. Extractive desulfurisation of gasoline with tetrabutyl ammonium chloride-based deep eutectic solvents. *Separation Science and Technology* **2016**, *51*, 1336–1343.
- (108) Jeschke, P.; Nauen, R. Neonicotinoids—from zero to hero in insecticide chemistry. *Pest Management Science* **2008**, *64*, 1084–1098.
- (109) Sánchez-Bayo, F.; Goulson, D.; Pennacchio, F.; Nazzi, F.; Goka, K.; Desneux, N. Are

- bee diseases linked to pesticides? — A brief review. *Environment International* **2016**, *89-90*, 7–11.
- (110) Jactel, H.; Verheggen, F.; Thiéry, D.; Escobar-Gutiérrez, A. J.; Gachet, E.; Desneux, N. Alternatives to neonicotinoids. *Environment International* **2019**, *129*, 423–429.
- (111) Thompson, D. A.; Lehmler, H.-J.; Kolpin, D. W.; Hladik, M. L.; Vargo, J. D.; Schilling, K. E.; LeFevre, G. H.; Peeples, T. L.; Poch, M. C.; LaDuca, L. E.; Cwiertny, D. M.; Field, R. W. A critical review on the potential impacts of neonicotinoid insecticide use: current knowledge of environmental fate, toxicity, and implications for human health. *Environ. Sci.: Processes Impacts* **2020**, *22*, 1315–1346.
- (112) Mahai, G.; Wan, Y.; Xia, W.; Wang, A.; Shi, L.; Qian, X.; He, Z.; Xu, S. A nationwide study of occurrence and exposure assessment of neonicotinoid insecticides and their metabolites in drinking water of China. *Water Research* **2021**, *189*, 116630.
- (113) De Gisi, S.; Lofrano, G.; Grassi, M.; Notarnicola, M. Characteristics and adsorption capacities of low-cost sorbents for wastewater treatment: A review. *Sustainable Materials and Technologies* **2016**, *9*, 10–40.
- (114) Zheng, X.; He, L.; Duan, Y.; Jiang, X.; Xiang, G.; Zhao, W.; Zhang, S. Poly(ionic liquid) immobilized magnetic nanoparticles as new adsorbent for extraction and enrichment of organophosphorus pesticides from tea drinks. *Journal of Chromatography A* **2014**, *1358*, 39–45.
- (115) Florindo, C.; Branco, L.; Marrucho, I. Development of hydrophobic deep eutectic solvents for extraction of pesticides from aqueous environments. *Fluid Phase Equilibria* **2017**, *448*, 135–142, Deep Eutectic Solvents.
- (116) Arnold, T.; Jackson, A. J.; Sanchez-Fernandez, A.; Magnone, D.; Terry, A. E.;

- Edler, K. J. Surfactant Behavior of Sodium Dodecylsulfate in Deep Eutectic Solvent Choline Chloride/Urea. *Langmuir* **2015**, *31*, 12894–12902, PMID: 26540438.
- (117) Atri, R. S.; Sanchez-Fernandez, A.; Hammond, O. S.; Manasi, I.; Douth, J.; Telam, J. P.; Edler, K. J. Morphology Modulation of Ionic Surfactant Micelles in Ternary Deep Eutectic Solvents. *The Journal of Physical Chemistry B* **2020**, *124*, 6004–6014, PMID: 32551622.
- (118) Tang, X.; Koenig, P. H.; Larson, R. G. Molecular Dynamics Simulations of Sodium Dodecyl Sulfate Micelles in Water—The Effect of the Force Field. *The Journal of Physical Chemistry B* **2014**, *118*, 3864–3880, PMID: 24620851.

242,500 BEADS



CORRESPONDING TO
1,800,000 ATOMS

For Table of Contents Use Only. Synopsis: New CG models for DESs allow for larger scale simulations which offer more relevance for the development and testing of new sustainable solvents.